AD-A191 033 SOLUTION OF THE COMPRESSIBLE NAVIER-STOKES EQUATIONS OF MOTION BY CHEBYSH..(U) NAVAL RESEARCH LAB WASHINGTON DC L SAKELL 18 MAR 88 NRL-MR-6152 1/1

UNCLASSIFIED F/G 20/4 NL

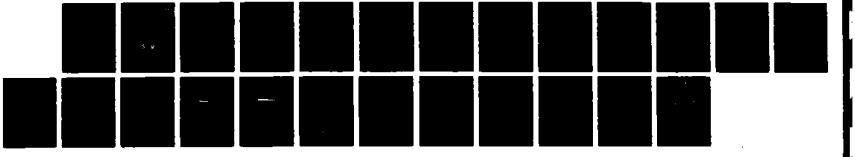

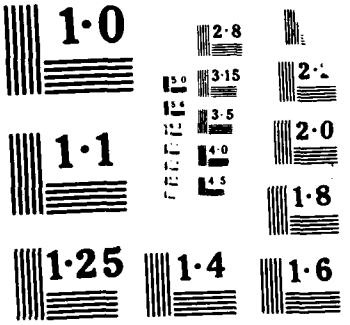
1·0
1·1
1·25
1·4
1·6
2·0
1·8

DTIC FILE COPY

Naval Research Laboratory
Washington, DC 20375-5000

NRL Memorandum Report 6152

Solution to the Compressible Navier-Stokes Equations of Motion by Chebyshev Polynomials for Laminar Shock-Boundary Layer Flow

LEONIDAS SAKELL

Center for Computational Physics Developments
Laboratory for Computational Physics and Fluid Dynamics

AD-A191 033

March 18, 1988

DTIC
ELECTE
APR 0 6 1988
S D
D

Approved for public release; distribution unlimited.

88 4 1 003

SECURITY CLASSIFICATION OF THIS PAGE

REPORT DOCUMENTATION PAGE

Form Approved
OMB No 0704-0188

1a REPORT SECURITY CLASSIFICATION UNCLASSIFIED	1b RESTRICTIVE MARKINGS AD-A191 033
2a SECURITY CLASSIFICATION AUTHORITY	3 DISTRIBUTION / AVAILABILITY OF REPORT Approved for public release; distribution unlimited
2b DECLASSIFICATION / DOWNGRADING SCHEDULE	
4 PERFORMING ORGANIZATION REPORT NUMBER(S) NRL Memorandum Report 6152	5 MONITORING ORGANIZATION REPORT NUMBER(S)
6a NAME OF PERFORMING ORGANIZATION Naval Research Laboratory 6b OFFICE SYMBOL (If applicable) Code 4440	7a NAME OF MONITORING ORGANIZATION Office of Naval Research
6c ADDRESS (City, State, and ZIP Code) Washington, DC 20375-5000	7b ADDRESS (City, State, and ZIP Code) Arlington, VA 22217
8a NAME OF FUNDING / SPONSORING ORGANIZATION Office of Naval Research 8b OFFICE SYMBOL (If applicable)	9 PROCUREMENT INSTRUMENT IDENTIFICATION NUMBER
8c ADDRESS (City, State, and ZIP Code) Arlington, VA 22217	10 SOURCE OF FUNDING NUMBERS PROGRAM ELEMENT NO / PROJECT NO / TASK NO / WORK UNIT ACCESSION NO

11 TITLE (Include Security Classification)
Solution to the Compressible Navier-Stokes Equations of Motion by Chebyshev Polynomials for Laminar Shock-Boundary Layer Flow

12 PERSONAL AUTHOR(S)
Sakell, Leonidas

13a TYPE OF REPORT	13b TIME COVERED FROM ____ TO ____	14 DATE OF REPORT (Year, Month, Day)	15 PAGE COUNT
		1988 March 18	24

16 SUPPLEMENTARY NOTATION

17 COSATI CODES			18 SUBJECT TERMS (Continue on reverse if necessary and identify by block number)
FIELD	GROUP	SUB-GROUP	Pseudospectral Chebyshev polynomials Navier-Stokes Compressible

19 ABSTRACT (Continue on reverse if necessary and identify by block number)

The time dependent, compressible, 2-D Navier-Stokes equations of motion are solved by full pseudo-spectral means. The flow solved for is a laminar oblique shock-boundary layer interaction. Comparison of the numerical surface pressure field with the experimental one is very good.

20 DISTRIBUTION / AVAILABILITY OF ABSTRACT	21 ABSTRACT SECURITY CLASSIFICATION
☒ UNCLASSIFIED/UNLIMITED ☐ SAME AS RPT ☐ DTIC USERS	UNCLASSIFIED
22a NAME OF RESPONSIBLE INDIVIDUAL Leonidas Sakell	22b TELEPHONE (Include Area Code) (202) 767-2457 22c OFFICE SYMBOL Code 4440

DD Form 1473, JUN 86

SECURITY CLASSIFICATION OF THIS PAGE

CONTENTS

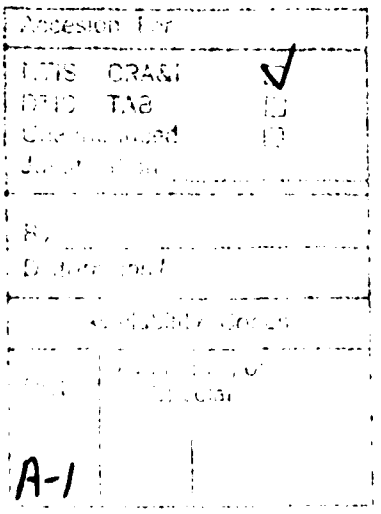

SOLUTION TO THE COMPRESSIBLE NAVIER-STOKES EQUATIONS OF MOTION BY CHEBYSHEV POLYNOMIALS FOR LAMINAR SHOCK-BOUNDARY LAYER FLOW

1. INTRODUCTION

Gottlieb et. al. (reference 1) applied pseudospectral methods to the solution of the one dimensional propagating shock wave problem. They utilized a low pass spectral filter which they developed together with a Shuman filter, applied to the flow on either side of the shock wave but not across the shock front itself. The shock location was determined by examination of the spectral coefficients. Since then, the present author has developed new techniques for use with pseudospectral methods which have greatly increased their utility in solving inviscid flows with single or multiple discontinuities. Pseudospectral methods have been used by the author to solve many classes of complicated time dependent compressible flows using the full Euler equations of motion (references 2 through 6). Results have shown that flow discontinuities such as shock waves or contact surfaces are properly resolved as sharp discontinuities. Solutions for transonic airfoil flows at subcritical and supercritical conditions (reference 6) were obtained more recently and proved that full pseudospectral computational methods could also successfully treat compressible inviscid flows about non-planar geometries. With the completion of the airfoil work, the author has shown that pseodospectral computational methods are fully suitable for solving any class of inviscid, time dependent, compressible flow using the Euler equations of motion.

The next logical step is to turn to the full viscous equations of motion namely, the Navier-Stokes equations. Orszag is the most notable in the field when one considers stability and transition analyses of incompressible hydrodynamic boundary layer and channel flows (reference 7 for example). He was the first to apply pseudospectral methods, treating flow stability problems for laminar hydrodynamic boundary layers. However, no work has as yet been done for compressible flows. Even when one considers the solution to compressible external flows, pseudospectral methods have not been used

Manuscript approved December 30, 1987.

at all due to difficulties in resolving discontinuities. The present work remedies this difficulty and shows that when techniques developed by the author are implemented, full pseudospectral computational methods can successfully solve viscous, time dependent compressible flows with multiple discontinuities and flow separation.

2. GOVERNING EQUATIONS

The full two-dimensional, time dependent, compressible Navier-Stokes equations of motion cast in conservation law form are shown below.

$$\frac{\partial \vec{U}}{\partial t} + \frac{\partial \vec{E}}{\partial x} + \frac{\partial \vec{F}}{\partial y} = 0, \tag{1}$$

where U , E and F are vectors whose elements are:

$$\vec{U} = \begin{vmatrix} \rho \\ \rho u \\ \rho v \\ e \end{vmatrix} \tag{2a}$$

$$\vec{E} = \begin{vmatrix} \rho u \\ \rho u^2 + \sigma_x \\ \rho uv + \tau_{xy} \\ (e + \sigma_x)u + \tau_{yx}v - \kappa \frac{\partial T}{\partial x} \end{vmatrix} \tag{2b}$$

$$\vec{F} = \begin{vmatrix} \rho v \\ \rho uv + \tau_{yx} \\ \rho v^2 + \sigma_y \\ (e + \sigma_y)v + \tau_{xy}u - \kappa \frac{\partial T}{\partial y} \end{vmatrix} \tag{2c}$$

and

$$\begin{aligned} \sigma_x &= p - \lambda(\frac{\partial u}{\partial x} + \frac{\partial v}{\partial y}) - 2\mu \frac{\partial u}{\partial x} \\ \tau_{xy} &= \tau_{yx} = -\mu(\frac{\partial u}{\partial y} + \frac{\partial v}{\partial x}) \\ \sigma_y &= p - \lambda(\frac{\partial u}{\partial x} + \frac{\partial v}{\partial y}) - 2\mu \frac{\partial v}{\partial y}, \\ \lambda &= -\frac{2}{3}\mu \end{aligned} \tag{2d}$$

$$\mu = \frac{T^{1.5}}{(T + 198.6)} x 10^{-8}$$

where σ_x ,σ_y are the normal stresses,τ_{xy} and τ_{yx} are the shear stresses, λ and μ are viscosity coefficients (Sutherland's relation is used since the present work deals with laminar flow) and κ is the coefficient of thermal conductivity. The pressure is obtained from the following

$$e = \frac{p}{(\gamma - 1)} + \frac{1}{2}\rho(u^2 + v^2), \tag{2e}$$

The physical flow variables are non-dimensionalized in the following manner.

$$\begin{aligned}
\bar{p} &= \frac{p}{\rho_1 U_1^2} \\
\bar{\rho} &= \frac{\rho}{\rho_1} \\
\bar{T} &= \frac{T}{(\frac{U_1^2}{R})} \\
\bar{u} &= \frac{u}{U_1} \\
\bar{v} &= \frac{v}{V_1} \\
\bar{\mu} &= \frac{\mu}{\mu_1}
\end{aligned} \tag{3}$$

The normal and shear stress terms are non-dimensionalized by the free stream pressure head, $(\rho_1 U_1^2)$. Subscript one denotes free stream properties upstream of the incident shock wave. With respect to non-dimensional flow variables, equation one becomes:

$$\frac{\partial \bar{U}}{\partial t} + \frac{\partial \bar{E}}{\partial x} + \frac{\partial \bar{F}}{\partial y} = 0 \tag{4a}$$

where

$$\bar{U} = \frac{1}{U_1} \begin{vmatrix} \bar{\rho} \\ \bar{\rho}\bar{u} \\ \bar{\rho}\bar{v} \\ \bar{e} \end{vmatrix} \tag{4b}$$

$$\bar{E} = \begin{vmatrix} \bar{\rho}\bar{u} \\ \bar{\rho}\bar{u}^2 + \bar{p} + \frac{2\bar{\mu}}{Re_1}[\frac{1}{3}(\frac{\partial \bar{u}}{\partial x} + \frac{\partial \bar{v}}{\partial y}) - \frac{\partial \bar{u}}{\partial x}] \\ \bar{\rho}\bar{u}\bar{v} - \frac{\bar{\mu}}{Re_1}[\frac{\partial \bar{u}}{\partial y} + \frac{\partial \bar{v}}{\partial x}] \\ (\bar{e} + \bar{\sigma}_x)\bar{u} + \bar{\tau}_{yx}\bar{v} - \frac{\gamma\bar{\mu}}{(\gamma-1)PrRe_1}\frac{\partial \bar{T}}{\partial x} \end{vmatrix} \tag{4c}$$

$$\bar{F} = \begin{vmatrix} \bar{\rho}\bar{v} \\ \bar{\rho}\bar{u}\bar{v} - \frac{\bar{\mu}}{Re_1}(\frac{\partial \bar{u}}{\partial y} + \frac{\partial \bar{v}}{\partial x}) \\ \bar{\rho}\bar{v}^2 + \bar{p} + \frac{2\bar{\mu}}{Re_1}[\frac{1}{3}(\frac{\partial \bar{u}}{\partial x} + \frac{\partial \bar{v}}{\partial y}) - \frac{\partial \bar{v}}{\partial y}] \\ (\bar{e} + \bar{\sigma}_y)\bar{v} + \bar{\tau}_{xy}\bar{u} - \frac{\gamma\bar{\mu}}{(\gamma-1)PrRe_1}\frac{\partial \bar{T}}{\partial y} \end{vmatrix} \tag{4d}$$

with the Prandtl number Pr defined by,

$$Pr = \frac{\mu C_p}{\kappa} \tag{4e}$$

This completes the non-dimensionalization of the physical flow variables and the conversion of the Navier Stokes equations to non-dimensional physical flow variables. However, it still remains to transform these equations into a suitable computational space. This is discussed below. Several coordinate transformations are applied to generate an appropriate distribution of points in the flow field. Appropriate here means many points in regions of large gradients and simultaneously few points in regions of small gradients. The final computational coordinates are obtained using a sequence of four coordinate transformations. Namely,

$$(x, y) \rightarrow (\xi, \eta) \rightarrow (\xi, \zeta) \rightarrow (\bar{\xi}, \bar{\zeta}) \tag{5}$$

where

$$x = A_x\xi\frac{1 - C_1\alpha\xi^2}{(1 - \xi^2)^\alpha} - C_3[1 - \frac{\xi^2 - \xi_{ic}{}^2}{\xi_1{}^2 - \xi_{ic}{}^2}] \tag{6a}$$

$$-x_{max} \leq x \leq x_{max} \rightarrow -\xi_1 \leq \xi \leq \xi_2$$

$$\bar{\xi} = 2[\frac{\xi - \xi_1}{\xi_2 - \xi_1}] - 1 \tag{6b}$$

$$-1 \leq \bar{\xi} \leq +1$$

and

$$y = A_y \eta \frac{1 - C_1 \alpha \eta^2}{(1 - \eta^2)^\alpha} \tag{7a}$$

$$0 \leq y \leq y_{max} \rightarrow 0 \leq \eta \leq \eta_{max}$$

$$\zeta = \frac{\eta - \eta_{min}(\bar{\xi})}{\eta_{max} - \eta_{min}(\bar{\xi})} \tag{7b}$$

$$0 \leq \zeta \leq \zeta_{max}$$

$$\bar{\zeta} = 2(\frac{\zeta}{\zeta_{max}}) - 1 \tag{7c}$$

$$-1 \leq \bar{\zeta} \leq +1$$

The terms C_1, C_3, A_x,A_y and , α are transformation clustering constants which affect the distribution of points in the computational and physical domains. The final form of the Navier Stokes equations becomes,

$$\tilde{U}_t + \tilde{E}_{\bar{\xi}} + \tilde{F}_{\bar{\zeta}} + \tilde{H} = 0 \tag{8}$$

where

$$\tilde{U} = \bar{U}$$

$$\tilde{E} = \bar{E}\bar{\xi}_x$$

$$\tilde{F} = \bar{E}\bar{\zeta}_{\bar{\xi}}\bar{\xi}_x + \bar{F}\bar{\zeta}_\eta\eta_y$$

$$\tilde{H} = -\bar{E}(\bar{\xi}_x)_{\bar{\xi}} - [\bar{E}(\bar{\zeta}_{\bar{\xi}}\bar{\xi}_x)_{\bar{\zeta}} + \bar{F}(\bar{\zeta}_\eta\bar{\eta}_y)_{\bar{\zeta}}]$$

All spatial derivatives appearing in equation 8 are calculated by pseudospectral means. In the present work this involves the use of chebyshev polynomials. The time derivative $\tilde{U}_t$ appearing in equation 8 is evaluated using finite differences. Specifically, the Adams Bashforth algorithm is used. The resultant difference form of equation 8 is given by,

$$\tilde{U}^{t+\delta t} = \tilde{U}^t + \frac{3}{2}\delta t[\frac{\partial\tilde{E}}{\partial\bar{\xi}}]^t - \frac{1}{2}\delta t[\frac{\partial\tilde{E}}{\partial\bar{\xi}}]^{t-\delta t} + \frac{3}{2}\delta t[\frac{\partial\tilde{F}}{\partial\bar{\zeta}}]^t - \frac{1}{2}\delta t[\frac{\partial\tilde{F}}{\partial\bar{\zeta}}]^{t-\delta t} - \tilde{H}^t + D_{i,j} \quad (9)$$

The term $D_{i,j}$ is an artificial viscosity. In the present work a fourth order artificial viscosity is utilized and is computed using finite differences. The finite difference representation is shown below.

$$D_{i,j} = \mu_x + \mu_y \quad (10)$$

where

$$\mu_x = -D_x[\tilde{U}_{i,j+2} + \tilde{U}_{i,j-2} - 4(\tilde{U}_{i,j+1} + \tilde{U}_{i,j-1}) + 6\tilde{U}_{i,j}]$$

$$\mu_y = -D_y[\tilde{U}_{i+2,j} + \tilde{U}_{i-2,j} - 4(\tilde{U}_{i+1,j} + \tilde{U}_{i-1,j}) + 6\tilde{U}_{i,j}]$$

The terms D_x and D_y are smoothing constants.

3. PSEUDOSPECTRAL METHODS

Pseudospectral solution techniques involve the use of series of functions to represent the global properties of a flow field and its spatial derivatives. In the present work Chebyshev polynomials are used. They are represented by $T_n(x)$ where

$$T_n(x) = \cos[n\arccos(x)] \tag{11}$$

or

$$T_n(\theta) = \cos[n\theta] \tag{12a}$$

where

$$\theta = \arccos(x) \tag{12b}$$

A function of a single spatial variable and time such as F(x,t) may be represented as

$$F(x,t) = \sum_{n=0}^{N} A_n(t) T_n(x) \tag{13}$$

The time dependence is represented entirely in the spectral coefficients $A_n(t)$ while, the spatial dependence is represented in the Chebyshev polynomials $T_n(x)$. The Chebyshev polynomials are evaluated at discrete points x_j where

$$x_j = \cos[\frac{\pi j}{N_x}] \tag{14}$$

where N_x is the total number of modes used to represent the spatial variation of the function F(x,t). The spatial derivative of the function F(x,t) is represented as

$$\frac{\partial F(x_j,t)}{\partial x} = \sum_{n=0}^{N_x} A_n(t)^{(1)} T_n(x_j) \tag{15a}$$

where

$$A_n{}^{(1)}(t) = \frac{2}{C_n} \sum_{p=n+1}^{N_x} p A_p(t) \tag{15b}$$

and

$$p + n = odd$$

$$C_0 = 2$$

$$C_{n>0} = 1$$

The $A_n{}'s$ are determined from equation thirteen. Inverse FFT's are used to obtain the $A_n{}'s$ from the known functional values F(x,t) at the known collocation points x_j. The spectral coefficients of the spatial derivative , $A_n{}^{(1)}$, are determined from the recurrence relation equation 15b. Direct FFT's are used to evaluate the sum in equation thirteen to obtain the functional values at t+δt. The low pass spectral filter developed by Gottlieb at ICASE is used to damp spectral oscillations. It is shown below.

$$e^{-\alpha \bar{K}^4} \tag{16}$$

with

$$\bar{K} = \frac{K - K_0}{K_{max} - K_0}$$

$$K_0 = \frac{5}{6} K_{max}$$

where K is the spectral wavenumber and K_{max} is the maximum wavenumber corresponding to the total number of collocation points.

4. RESULTS

The following free stream conditions were selected to match one of the wind tunnel experiments reported in reference 8. An experimentally measured surface pressure distribution is included in the above reference so that a direct comparison can be made between the experimental and numerical distributions. The free stream mach and unit Reynolds numbers are 2.05 and 695,000 per foot respectively. The free stream Prandtl number is 0.71. The incident shock wave was generated by a six degree wedge. The physical extent of the computational domain is $0 \leq y \leq 0.3$ foot and $-0.2 \leq x \leq +0.2$. No attempt was made to select an optimum shape for the computational boundary , such as alligning constant coordinate lines with the incident and reflected shock wave system, since the purpose of the present work is to determine whether pseudospectral computational techniques can actually solve the full time dependent, compressible Navier-Stokes equations of motion with discontinuities. The flat plate surface lies in the range $-.14 \leq x \leq +0.2$ so that several grid points lie ahead of the plate leading edge. Sixty four modes each were used to represent the flow field in the x and y directions. The physical space computational boundary is shown in Figure 1 along with constant coordinate lines showing the degree of clustering in both the x and y directions. As can be seen, points are highly clustered in the y direction at the surface. This was done to properly resolve the flow separation zone and attendent shock structure which arises very close to the plate surface. Points are only mildly clustered along the x-direction since an airfoil coordinate transformation which clusters points about the leading and trailing edges was used with the clustering parameters detuned. The inflow boundary conditions were to keep all flow variables fixed because of supersonic inflow. Along the upper boundary flow variables were held fixed at post incident shock conditions since for the flow considered the reflected shock does not extend to the upper boundary location. At the outflow boundary conditions at each point were set to those at the next upstream point (zero'th order extrapolation) throughout the calculation. Along the bottom of the computational boundary either a plane of symmetry or wall surface was present. Reflective boundary conditions were used at points ahead plate leading edge namely, $u_{i,1} = u_{i,2}$. On the plate surface, $u_{i,1} = -u_{i,2}$. Also, along the entire bottom boundary $v_{i,1} = -v_{i,2}$, $p_{i,1} = p_{i,2}$ and $\epsilon_{i,1} = \epsilon_{i,2}$, with ϵ denoting specific internal energy. This last condition being applied along the plate surface since the case being treated is an adiabatic wall. The time step size was determined from the following.

$$\delta t_\xi = \frac{CN\Delta\xi_{min}^2}{|\sigma_\xi|_{max}\Delta\xi_{min} + \frac{2}{Re}} \tag{17a}$$

$$\delta t_{\bar{\zeta}} = \frac{CN\Delta\bar{\zeta}_{min}{}^{2}}{|\sigma_{\bar{\zeta}}|_{max}\Delta\bar{\zeta}_{min} + \frac{2}{Re_1}} \tag{17b}$$

$$\delta t = [\Delta t_{\bar{\xi}}, \Delta t_{\bar{\zeta}}]_{min} \tag{17c}$$

For results presented herein the courant number CN was held fixed at 2.5. No attempt was made to replace $\Delta\bar{\xi}_{min}$ or $\Delta\bar{\zeta}_{min}$ with the actual respective values at the points of maximum eigenvalue. The flowfield was initialized in two steps. First, the exact euler shock structure (incident and reflected) including post shock zones was put in. Figure 2 shows the initial shock system. This system is overlayed on the constant grid lines plot to show the relative grid resolution over the entire shock system in Figure 3. The second step was to put in a boundary layer field using a blasius velocity profile and the Crocco relation to obtain the density profile at constant pressure at each point along the plate surface. The pseudospectral code used to obtain the present results was run on the NRL CRAY XMP/12. The code takes 0.75 cpu second per iteration at a grid resolution of 64 by 64. The solution converged in 25,000 iterations or a little over five cpu hours. No optimization of any kind was employed since the purpose of this work was to determine if pseudospectral techniques could successfully solve the compressible Navier-Stokes equations. Pressure contours of the entire computational field are shown in Figure 4. There are no oscillations in the field. The incident shock is slightly smeared for several reasons. First, the grid system is not shock alligned. Second, the x-direction grid resolution is only moderate. Finally, at a courant number of 2.5 the magnitude of the artificial viscosity coefficients required for stability is relatively large to that required to keep the shock waves stable. This last condition is primarily responsible fro the shock smearing. With a courant number of 0.7 the thickness of the shock is only one third of that shown in the figures herein included. However, the penalty that one incurs for the reduction of shock smearing is an increase on CPU time. For the courant numbers thus mentioned, the CPU time would be increased by almost a factor of four. It was deemed more important for the present work to obtain a converged solution while minimizing the CPU time. An alternative would be to run at maximum courant number untill convergence is almost reached and then reduce the courant number and dissipation constants to have the best of both worlds. The reflected shock wave has split into two compression fans. One is well above the separation zone, while the second is the re-compression fan at the point of re-attachment of the separated shear layer on the plate surface. A blowup of the wall region pressure contours ($0 \leq y \leq 0.08 foot$) is shown in Figure 5. Corresponding velocity vector and mass flow per unit area contours are shown in Figures 6 and 7. The separation zone is clearly evident. Comparison of the numerical and experimental surface pressure distributions can be made from Figure 8. The starting location of the separation zone is in good agreement with

the data. The experimentally measured plateau pressure non-dimensionalized by pre-impingement free stream pressure is 1.25. The numerical value is about 1.29 or a little more than three per cent higher. The re-compression point location is in very good agreement. The numerical solution value is 0.155 foot from the plate leading edge while the experimental value is 0.165 foot. The length of the separation zone from the present work is 0.09 foot or 1.08 inch. The actual length is about one inch as determined from a schlieren photograph. The height of the separation zone is about the same as the experimental value. (This is all that can be said since the schlieren photograph in reference 8 is too small to measure the separation height.) The numerical pressure distribution through the recompression point is more rounded than the sharp discontinuity of the experimentally obtained distribution. The sharpness is in part due to the larger spacing of the experimental data points compared to the numerical grid point spacing. Thereafter, the numerical solution is in excellent agreement with the experimental data, falling right on top of the experimental data points.

Vertical profile plots of density, u-velocity, energy and, mass flow per unit area are shown in Figures 9 through 12 for the full computational domain as well as for the wall region. The vertical extent is 0.30 and 0.01 foot respectively, while the horizontal range of the plots covers each of the x locations. The horizontal spacing of the lines is proportional to the grid spacing in the x-direction and is not equal to it. The change in horizontal location of any curve from its surface position is representative of the change in the magnitude of the flow variable being plotted from the surface value. There are no numerical oscillations present at the wall. The separation zone is clearly shown in Figure 10.

5. CONCLUSIONS

The present work has shown that pseudospectral computational techniques are indeed able to accurately solve the compressible Navier-Stokes equations for flows simultaneously including separation zones and shock waves. No numerical oscillations are present in the solution. It still remains to incorporate existing acceleration techniques as well as to develop new ones to reduce the large computer time required to obtain a converged solution to a more practical level. Work is currently proceeding along these lines.

6. ACKNOWLEDGEMENT

This work was sponsored by the Office of Naval Research.

7. REFERENCES

[1] Gottlieb, D.,Lustman, L., and Orszag, S., "Spectral Calculations of One-Dimensional Inviscid Compressible Flows", SIAM J., Vol. 2, No. 3, September, 1981.

[2] Sakell,L., "Pseudospectral Solution of One Dimensional and Two Dimensional Inviscid Flows with Shock Waves", NRL Memorandum Report 4892, August 6, 1982, also published in AIAA Journal, Vol. 22, No. 7, July,1984, pp 929-936.

[3] Sakell,L., "Solution to the Euler Equations of Motion by Pseudospectral Techniques", paper presented at the 10th IMACS World Congress on System Simulation and Scientific Computations, Montreal, Canada, August 1982.

[4] Sakell,L., "Chebyshev-Series Solutions to the 1-D and 2-D Euler Equations With Shock Waves",paper presented at the Symposium on Spectral Methods for Partial Differential Equations, ICASE, NASA Langley, August 1982.

[5] Sakell,L., "Pseudospectral Solution of Inviscid Flows with Multiple Discontinuities", NRL Memorandum Report 5147, August 17,1983. ADA132084

[6] Sakell,L., "Full Pseudospectral Solution to the Euler Equations of Motion for Airfoil Flow at Transonic Speeds", NRL Memorandum Report 5674, September 30, 1985.

[7] Patera, A. T., and Orszag S. A., "Transition and Turbulence in Planar Channel Flows", Cambridge Hydrodynamics Report Number 37, 1981.

[8] Barry, F. W., Shapiro, A. H. and Neumann, E.P., "The Interaction of Shock Waves with Boundary Layers on a Flat Surface", JAS, April 1951.

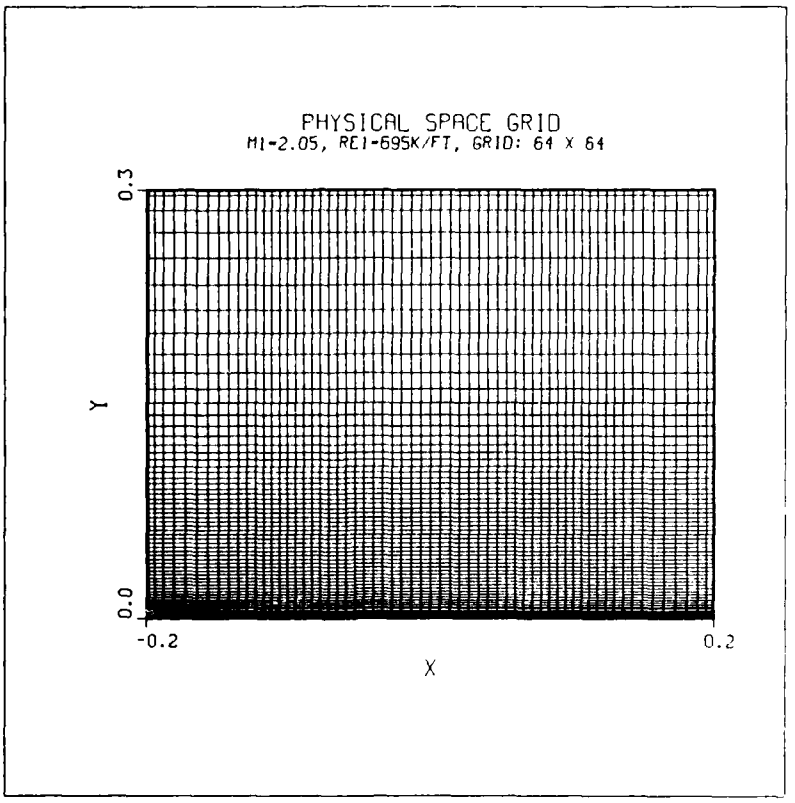

Figure 1 - Full Field Constant Coordinate Lines

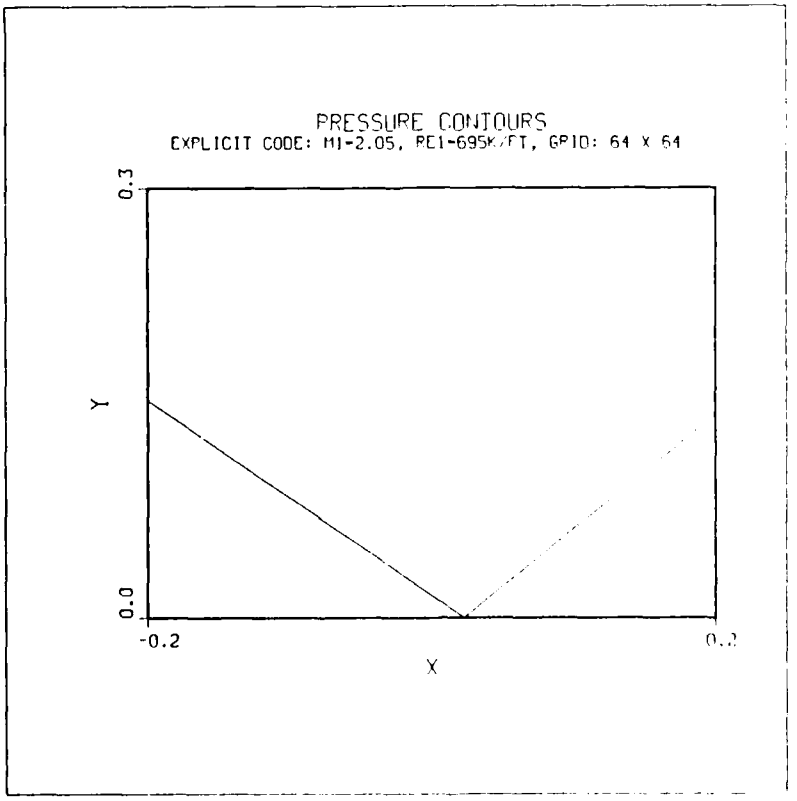

Figure 2 - Initial Euler Shock System

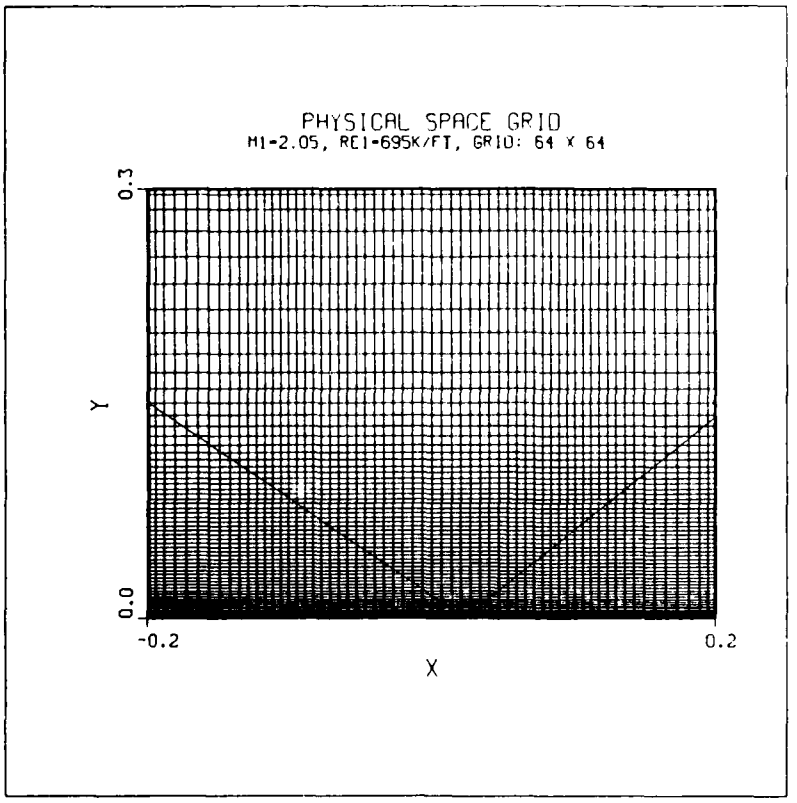

Figure 3 - Initial Shock System On Physical Space Grid

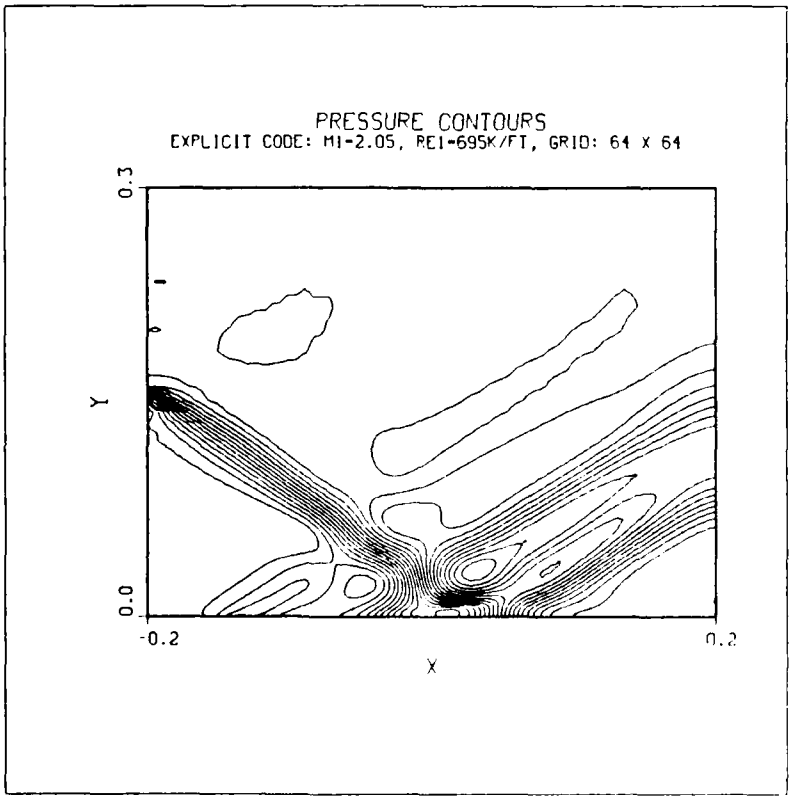

Figure 4 - Full Field Pressure Contours

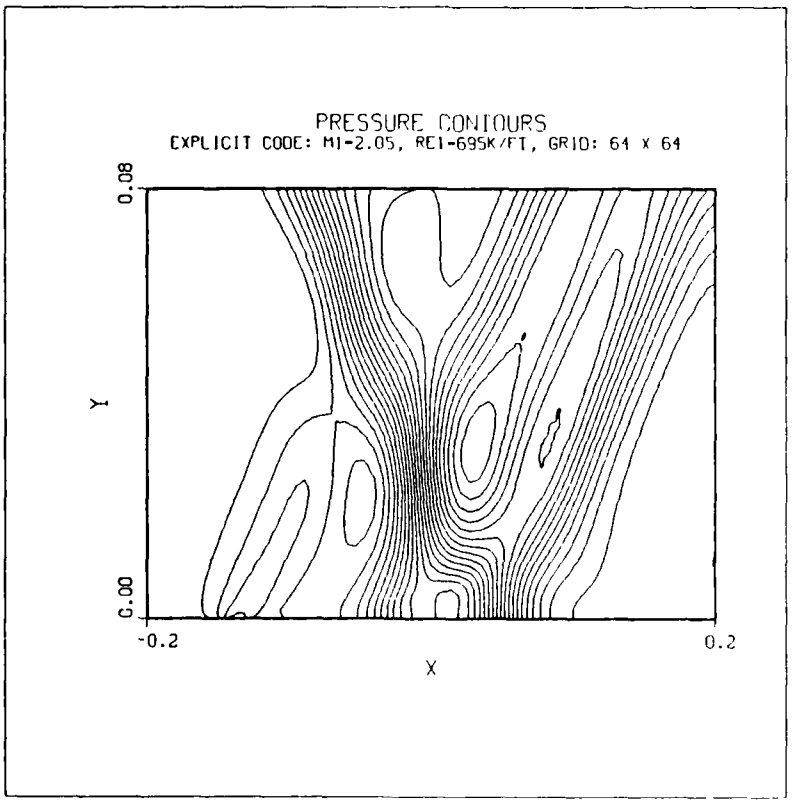

Figure 5 - Wall Region Pressure Contours

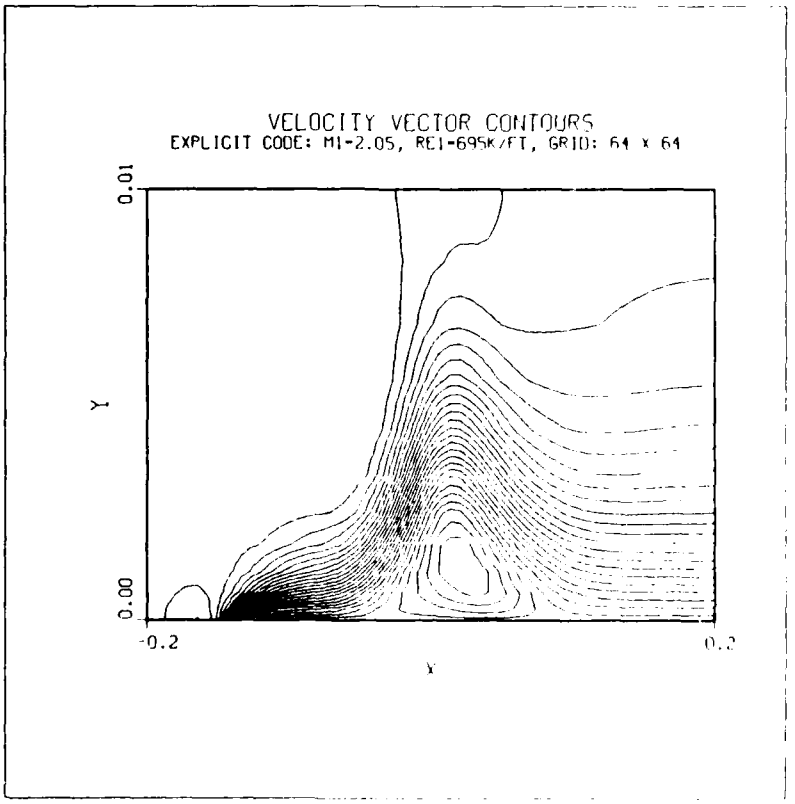

Figure 6 Wall Region Velocity Vector Contours

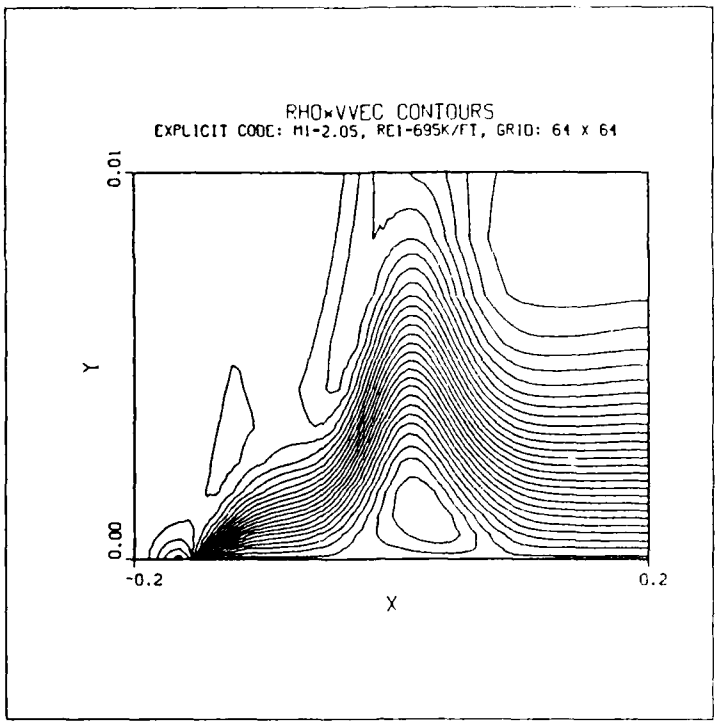

Figure 7 - Wall Region Unit Mass Flow Contours

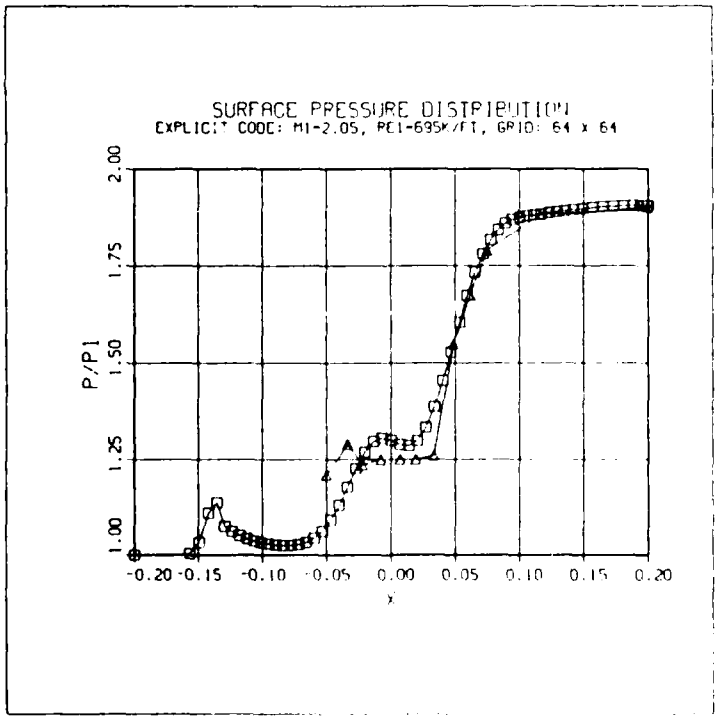

Figure 8 - Numerical vs. Experimental Surface Pressure Distribution (Square Symbols - Numerical Solution; Triangles-Experiment)

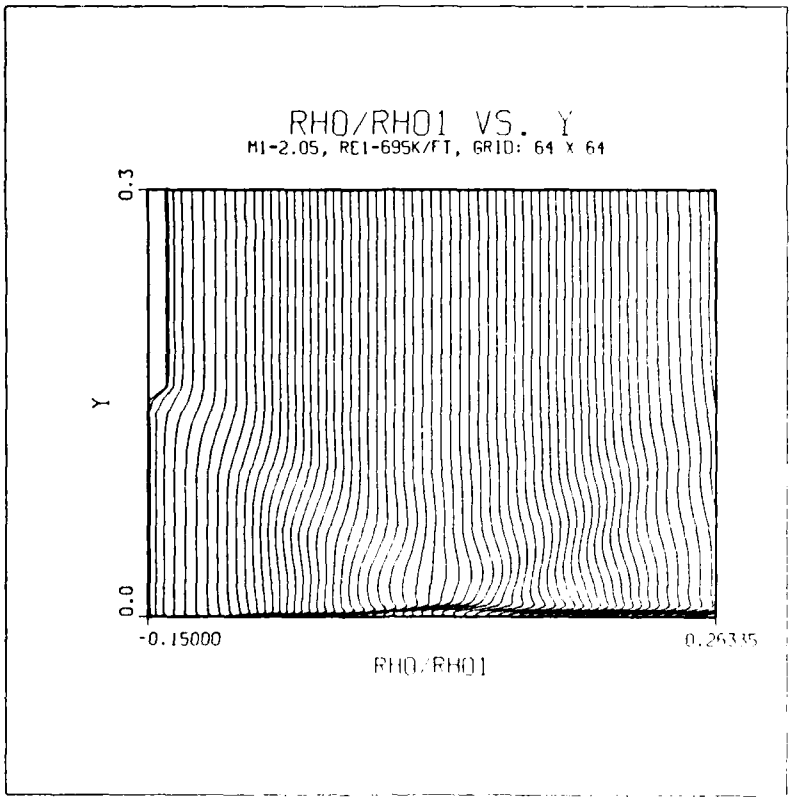

Figure 9a - Full Field Density Profiles

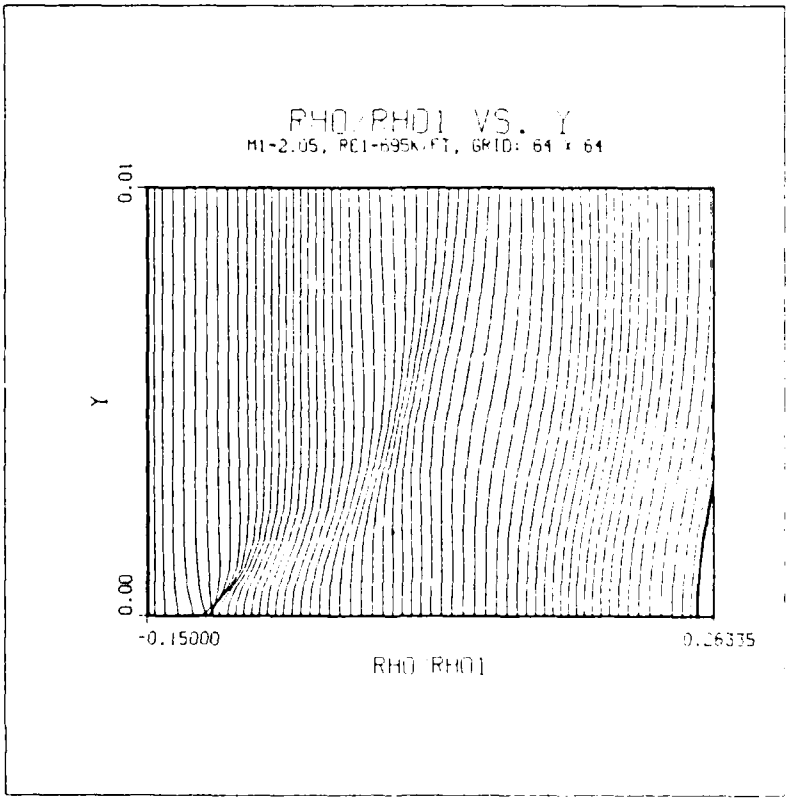

Figure 9b - Wall Region Density Profiles

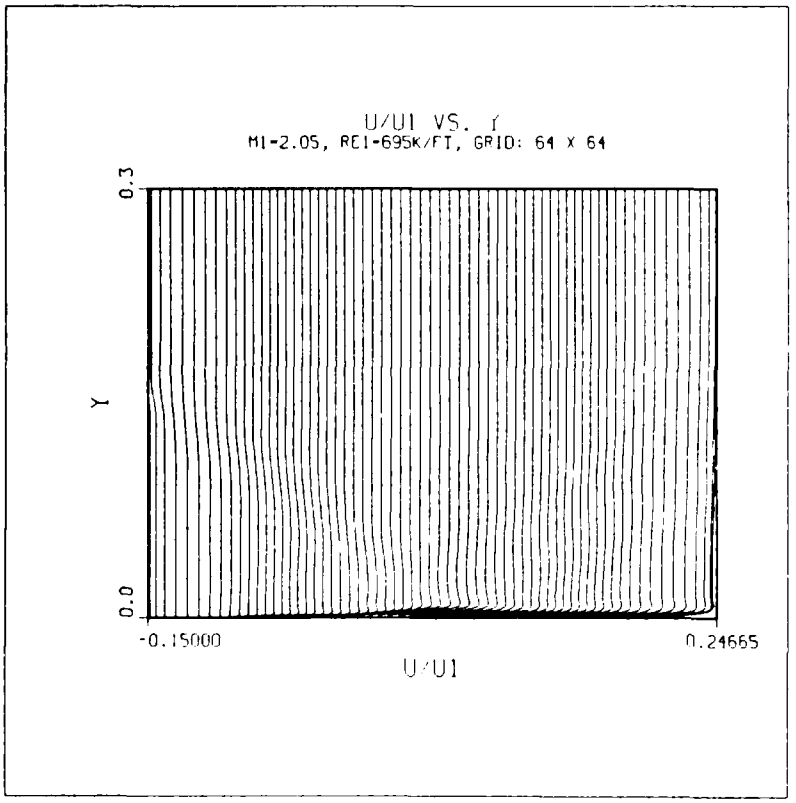

Figure 10a - Full Field Velocity Profiles

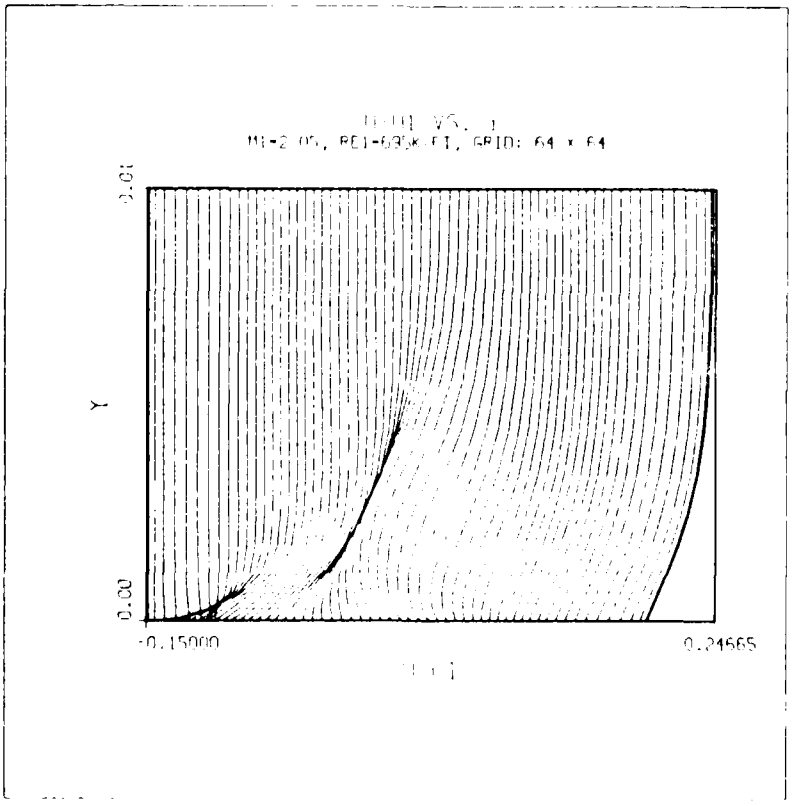

Figure 10b - Wall Region Velocity Profiles

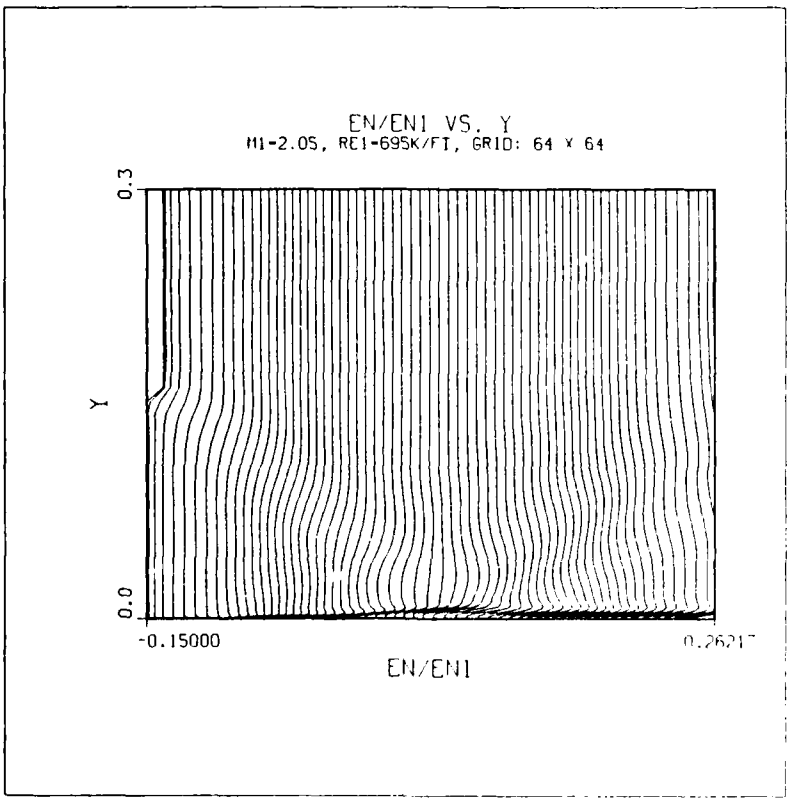

Figure 11a - Full Field Energy Profiles

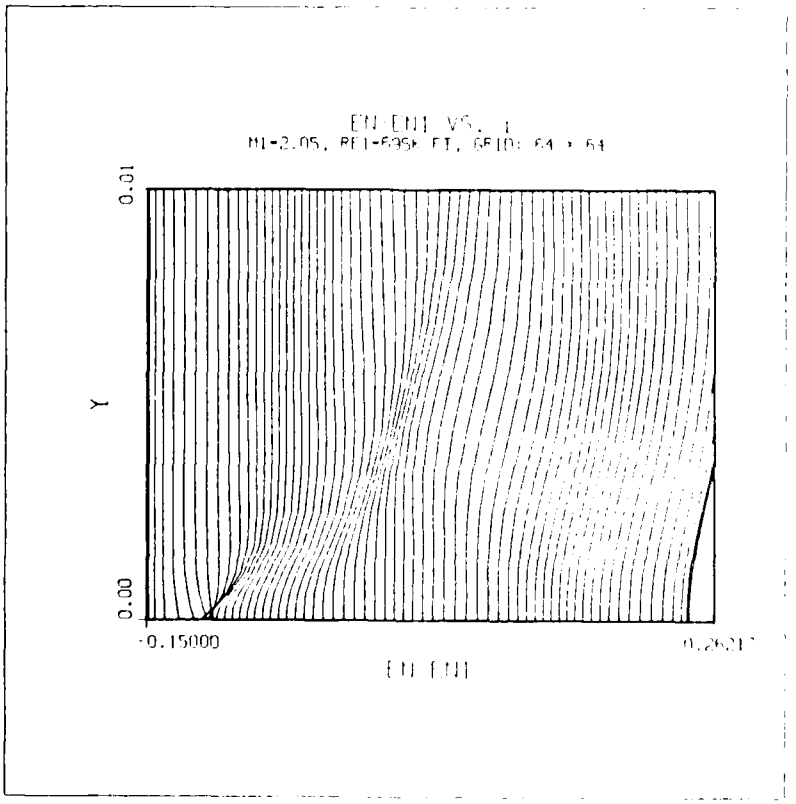

Figure 11b - Wall Region Energy Profiles

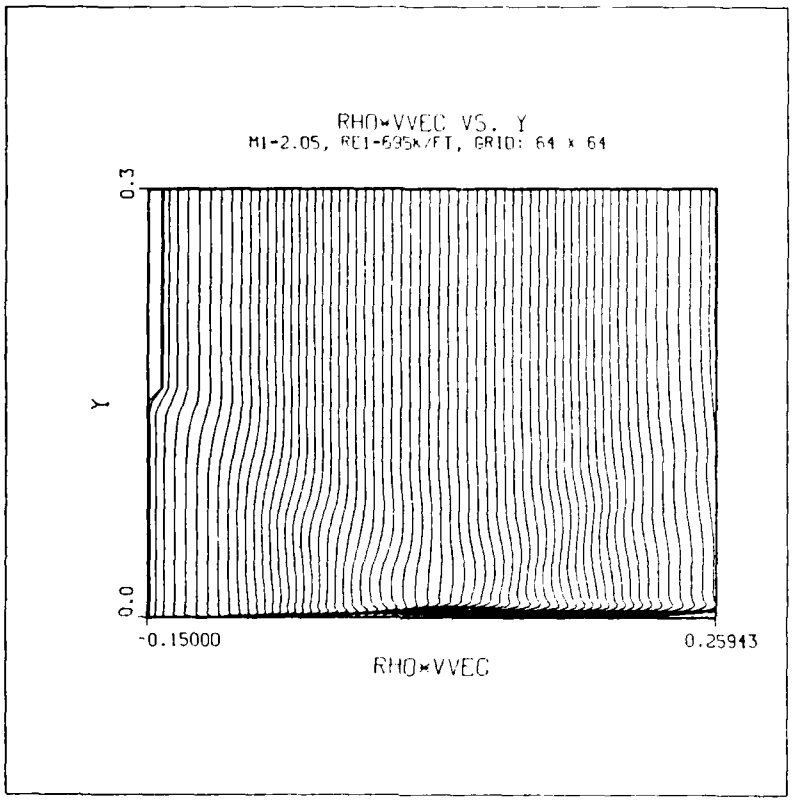

Figure 12a - Full Field Unit Mass Flow Profiles

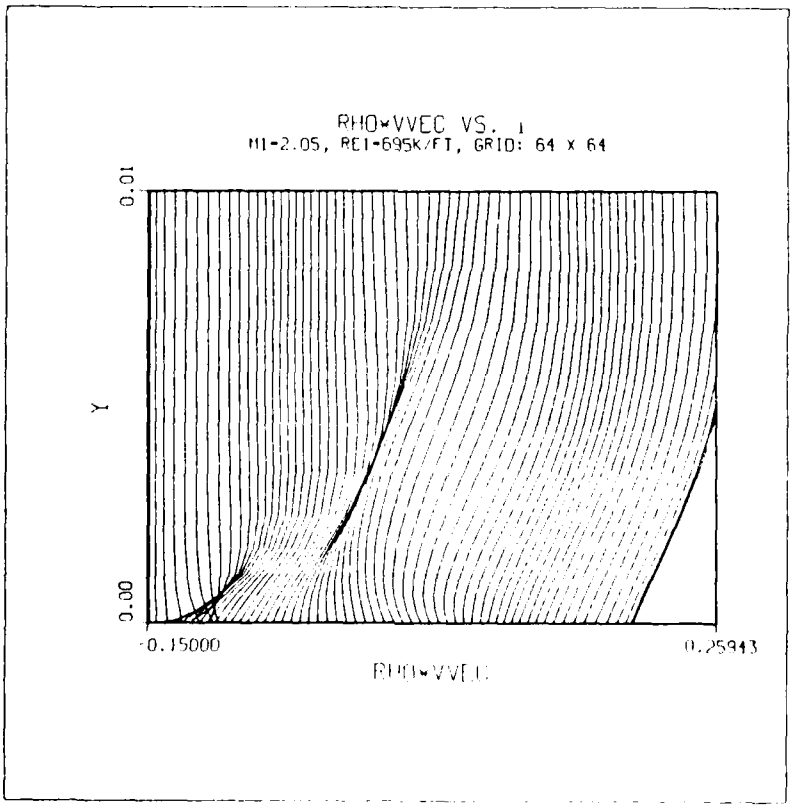

Figure 12b - Wall Region Unit Mass Flow Profiles

END

DATE

FILMED

5-88

DTIC